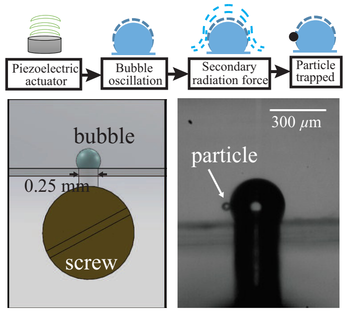

We quantitatively analyze the secondary radiation force of an acoustic bubble for particle trapping and release in a flow.

Journal Name

ARTICLE TYPE

Cite this: DOI: 10.1039/xxxxxxxxxx

Onset of Particle Trapping and Release via Acoustic Bubble†

Yun Chen,[a] Zecong Fang,[b] Brett Merritt,[b] Dillon Strack,[a] Jie Xu*[c] and Sungyon Lee*[a]

Received Date
Accepted Date

DOI: 10.1039/xxxxxxxxxx

www.rsc.org/journalname

Trapping and sorting of micro-sized objects is one important application of lab on a chip devices, with acoustic bubbles emerging as an effective, non-contact method. Acoustically actuated bubbles are known to exert a secondary radiation force (F_{SR}) on micro-particles and stabilize them on the bubble surface, when this radiation force exceeds external hydrodynamic forces that act to keep the particles in motion. While the theoretical expression of F_{SR} has been derived by Nyborg decades ago, no direct experimental validation of this force has been performed, and the relationship between F_{SR} and the bubble's ability to trap particles in a given lab on a chip device remains largely empirical. In order to quantify the connection between the bubble oscillation and resultant F_{SR}, we experimentally measure the amplitude of bubble oscillations that give rise to F_{SR} and observe the trapping and release of a single microsphere in the presence of the mean flow at the corresponding acoustic parameters using an acoustofluidic device. By combining well-developed theories that connect bubble oscillations to the acoustic actuation, we derive the expression for the critical input voltage that leads to particle release into the flow, in good agreement with the experiments.

1 Introduction

In the past two decades, microfluidics technology has become an emerging field that allows for precise control of fluids behavior at microscale[1,2]. Based on microfluidic technology, functional units, such as pumps, valves, sensors, and actuators, can be miniaturized and integrated onto a small microfluidic chip to form a lab on a chip system[3,4], which is now finding numerous applications in chemistry[5], biology[6–8], medicine[9,10], biotechnology[11], food science[12] and environmental engineering[13]. One of the most important functions in lab on a chip applications is the manipulation of micro-sized objects, including reagents, particles, cells, and microorganisms. Various methods have been developed for manipulation in a microfluidic environment. These methods often harness interactions between fluids and multi-physics, such as electric field[14–19], magnetic field[20–23], electromagnetic field[24–26], temperature field[27,28] and centrifugal force field[29,30]. In recent years, acoustics has also started to attract attention as an alternative source that can be utilized for manipulation of micro-objects in microfluidics, and a new term *acoustofluidics* has gained popularity in the research community[31,32]. Compared with other actuation techniques, acoustic methods offer many advantages, such as versatility, compactness, non-contact feature and relatively simple operation. However, the interactions between fluids and an acoustic field can be quite complex; Fig. 1 briefly summarizes possible acoustic effects that may arise when acoustics and fluids encounter at microscale.

Two types of interactions have been explored in the past. One is to directly use the interactions between objects and acoustic waves, which include surface waves[33,34] or bulk standing waves[35,36]. The other is to harness secondary acoustic effects in the vicinity of solid structures including microchambers[37] and sharp edges[38], or most often, microbubbles[39,40]. In particular, microbubbles oscillating in an acoustic field can be categorized into inertial or non-inertial types depending on the oscillation magnitude. Inertial bubble oscillation, or inertial cavitation, is very violent, unstable, and transient, resulting in liquid jetting in the case of the asymmetrical bubble collapse, or energy emitting via shock waves or light[41]. This particular mode of acoustic bubbles has been widely used in medical ultrasonics[42–45]. Non-inertial microbubble oscillation is much gentler with various stable oscillation modes that may be observed in the form of interfacial waves[46,47]. Non-inertial microbubbles may influence surrounding objects by generating microstreaming flows[48–50], or by exerting a secondary radiation force, F_{SR} [51,52].

Most bubble-based lab on a chip systems to date utilize non-inertial microbubbles, due to the fact that non-inertial microbubbles are more stable and can be easily controlled both spatially

[a] *Mechanical Engineering, Texas A & M University, College Station, TX 77840, USA. E-mail: sungyon.lee@tamu.edu*
[b] *Mechanical Engineering, Washington State Univeristy, Vancouver, WA 98686, USA.*
[c] *Mechanical Engineering, University of Illinois, Chicago, IL 60607, USA. E-mail: jiexu@uic.edu*

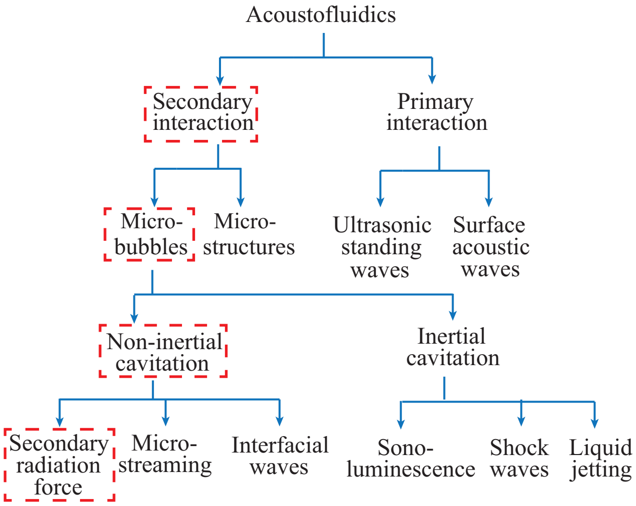

Fig. 1 Diagram showing different interactions between acoustic actuation and fluid flows. The microbubble oscillation caused by acoustic field is in the secondary interaction category. The oscillating bubble can impact the objects in the nearby field generating microstreaming flows and secondary radiation forces, F_{SR}. In this study, we focus on the effect of F_{SR}.

and temporally in a microfluidic environment. For example, the secondary radiation force from an oscillating bubble can be used to trap micro-objects, while the position of the bubble itself can be controlled by using electrowetting technique[53] or simply attaching the bubble to a traverse rod[54]. If an array of bubbles is fixed inside a microchannel and acoustically actuated, a trapping zone will form near the oscillating bubbles, which can be used to enrich, sort and manipulate *C. elegans* in a flow[55]. Moreover, if excited with maximized microstreaming flows, spatially arranged bubbles in a microchannel can be used as fixated transporters[56–59]. Other notable applications involving acoustic bubbles include enhanced mixing[60], pumping flow in a microchannel[61,62], switching particle pathlines[63], switching flow optical properties[64], assembling and driving microrotors[65], generating chemical gradients[66] and propelling objects[67,68].

Although applications of acoustic bubbles in lab on a chip systems have witnessed tremendous progress recently, the operating conditions of the experiments are largely determined empirically in most applications mentioned above, and there exists a lack of theoretical guidance for designing devices. Indeed, it has been shown that even for a simple straight 1D channel, the actual outcome of the acoustic actuation is difficult to predict using theoretical or numerical methods[69]. Therefore, for any given device, initial experimental validation is important for any further theoretical or modeling efforts. One particular area of acoustofluidics with the latest theoretical development is microstreaming flows[57,70–75], as both the microstreaming flow field and its effect on micro-sized objects have been resolved analytically in two-dimensional and quasi-three dimensional geometries. By contrast, while the theoretical expression of F_{SR} has been developed by Nyborg[76] and Doinikov[77], it has not been experimentally verified or implemented to directly quantify the bubble's ability to trap a given micro-object in microfluidic devices. For instance, Xu et al[55] and Neild et al[78] demonstrated trapping of microworms and microspheres, respectively, via acoustically actuated bubbles that exert secondary radiation forces. However, no measurement of bubble oscillations has been made to connect the amplitude of bubble oscillations to F_{SR}, then to the ability of bubbles to trap particles. The authors also reported the critical voltages at a given frequency that lead to particle trapping but offered no quantitative analysis that connects the critical acoustic parameters to F_{SR}.

In order to address this current lack of quantitative analysis of F_{SR}, we hereby present the combined experimental and theoretical studies on particle trapping and release via an acoustic bubble in a simple 1D microfluidic channel. This will serve as an important first step towards more comprehensive future studies. Experimentally, we quantify the bubble's ability to stabilize a particle in two ways: first, by measuring the critical acoustic input at which a pre-loaded particle is released into the flow (Exp A); secondly, by measuring the critical acoustic voltage and frequency at which a particle is directed towards the bubble and is stabilized (Exp B). The corresponding amplitudes of bubble oscillations that give rise to F_{SR} are also measured. Furthermore, to isolate the effects of F_{SR} from all other forces acting on the particle, we keep the flow rate inside the channel constant to ensure that the relative effects of microstreaming flows may be neglected in our study. In addition, we combine the well-developed theories that connect bubble oscillations yielding F_{SR} to the acoustic actuation to theoretically derive the critical voltage.

Following the experimental method and image processing in Section 2, experimental results are reported in Section 3.1, consisting of the bubble oscillation magnitudes and the corresponding behavior of the microsphere at given voltages and frequencies. Sections 3.2 and 3.3 include the theoretical analysis to calculate the critical input voltage that leads to the particle release into the mean flow, in reasonable agreement with the experiments. The summary and future directions are given in Section 4.

2 Methods and Materials

2.1 Experimental setup

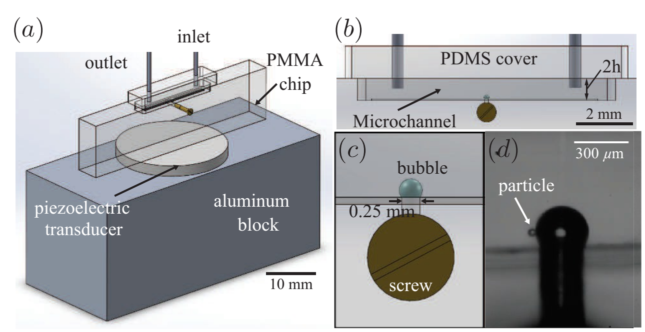

Fig. 2 (a) A perspective view of the device: the piezoelectric transducer is sandwiched between the transparent PMMA chip and an aluminum block. (b) A side view of the chip: the microchannel is milled on top of the chip. DI water is injected from the inlet and the spherical bubble is constrained on the bottom of the channel; (c) A miniature screw is used to control the bubble volume; (d) Once the piezoelectric transducer is excited, the bubble starts oscillating and generates a secondary radiation force to trap particles.

The experimental apparatus used in this study includes a transparent microfluidic chip, a piezoelectric transducer, and an aluminum block base, as shown in Fig. 2(a). The microfluidic channel (depth 2.79 mm $\times$ height 1.35 mm $\times$ length 14.01 mm) has been micro-milled out of PMMA and is sealed with PDMS and plastic sheets, with two flat needles (Lab Express Management) used as an inlet and an outlet. The channel also consists of a cylindrical cavity with diameter of 254 μm which is treated with superhydrophobic coating (Rain-X) to serve as a pre-defined site of bubble formation and stabilization[79]. An additional cylindrical cavity is drilled from the side to incorporate a miniature screw to actively control the bubble volume and is sealed by ultrasound gel (Aquasonic 100, Parker Laboratories), as shown in Fig. 2(c).

In our experiment setup, an air bubble forms automatically inside the cavity and remains stable when the solution with polystyrene microspheres (25-30 μm radius, Thermo Fisher Scientific) is introduced into the main channel through a syringe pump at a constant flow rate of 4 mL/min (NE-1000, New Era Pump Systems). Following the bubble formation, the screw is actively adjusted to achieve the desired bubble radius, typically in the range of 140 -160 μm. We use a piezoelectric transducer (20 mm $\times$ 2 mm) sandwiched between the PMMA chip and an aluminum block to excite the channel periodically using a function generator (DG1022, RIGOL Technologies) and an amplifier (7602M, Krohn-Hite). The driving frequency, f, ranges from 20 kHz to 36 kHz with an increment of 1 kHz, while the driving voltage, V, is varied from 10 V to 190 V at each frequency.

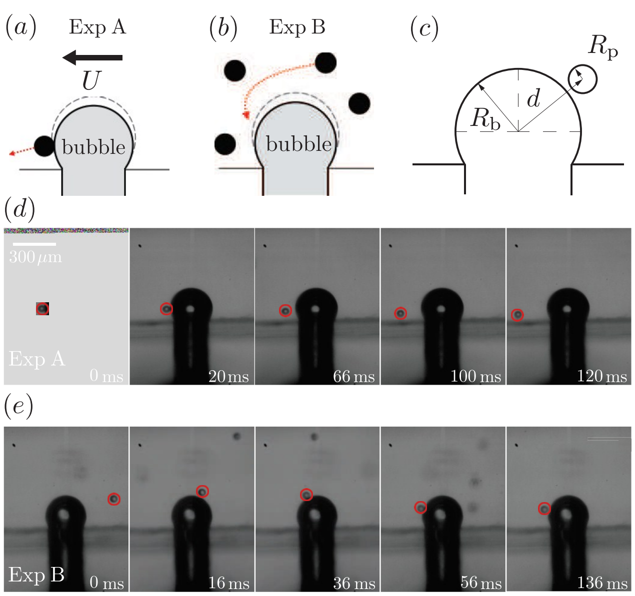

Fig. 3 (a) In Exp A, the particle is first trapped on the surface of the bubble. The critical voltage, V_c, at which the particles are released is recorded as the voltage is decreased for given frequency, f. (b) In Exp B, we measure the critical voltage, V_c, at which an acoustic bubble is able to trap particles originally in motion for varying f. (c) Here R_b and R_p are the radii of the bubble and particle, respectively, while d is the center-to-center distance between the particle and bubble. Images depicting particle trajectories are included in (d) and (e), respectively.

Two sets of experiments are conducted to quantify threshold acoustic parameters for particle trapping and release, as depicted in Fig. 3 (a) and 3 (b). In the first set (Exp A), we observe particles that have been stabilized onto the bubble surface at a high voltage being released into the external flow as the voltage is decreased. The critical voltage, V_c, at which the particles are released is recorded for a given frequency, f. In the second set (Exp B), we measure the critical voltage, V_c, at which an acoustic bubble is able to trap particles originally in motion for varying f. Image sequences of the particle release and trapping processes in Exp A and Exp B are shown in Fig. 3 (d) and (e), respectively. The experiments are recorded with a high-speed camera (Phantom Miro M310, Vision Research) from the side of the microchannel. For each experiment at given V and f, the interaction between the bubble and particle is captured at 1000 fps (240 $\times$ 320 pixels) to produce images in Fig. 3 (d)-(e), while the bubble oscillations are recorded at 120171 fps (128 $\times$ 128 pixels) with resultant images shown in Fig. 4 (a)-(b).

2.2 Data analysis

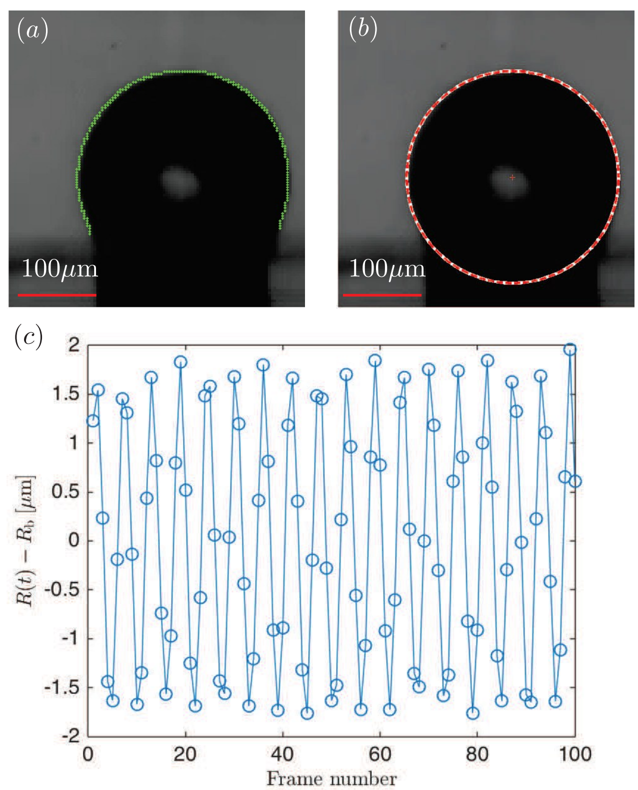

Fig. 4 (a) The edge of the bubble is first detected using Matlab Canny function. (b) The least square error method is used to find a circle that best fits the edge. (c) The plot shows the displacement of an oscillation bubble versus frame number at 21kHz and 190V calculated using fitted circle.

To measure the bubble oscillation amplitude, we use a MATLAB Canny function to detect the edge of the oscillating bubble as shown in Fig. 4 (a). Once the coordinate of the bubble edge has been determined, the least square error method is used to find a circle that best fits the edge (Fig. 4 (b)). Fig. 4 (c) shows one example of the oscillation displacement at 21 kHz and 190 V as a function of the frame number calculated using the instantaneous bubble radius, $R(t)$, minus the equilibrium bubble radius $R_b = 152.5\mu$m over 100 frames. The bubble amplitude is subsequently calculated by averaging over local maxima of $|R(t) - R_b|$. The consistency and periodicity of the displacement in Fig. 4 (c) demonstrate the effectiveness of our data analysis method.

3 Results

3.1 Experimental Data

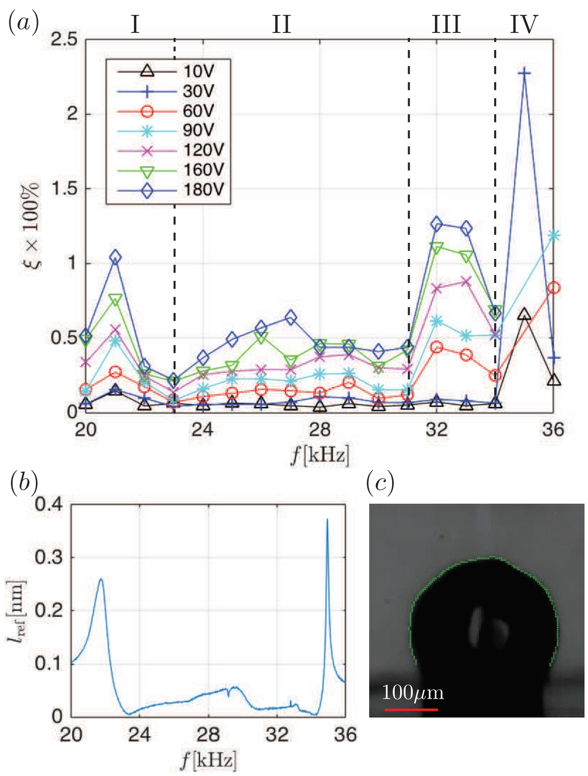

Fig. 5 (a) Dimensionless bubble amplitude ξ as a function of frequency f at various voltage. The plot shows that the magnitude of the oscillation amplitude generally increases with V but varies nonlinearly with f. We divide the plot into 4 different regimes depending on behavior of amplitude as a function of voltage. (b) Device vibration amplitude l_{ref} as a function of frequency at 3 V. The plot shows two peaks at 21 kHz and 35 kHz. (c) The snapshot of the oscillating bubble excited at 35 kHz shows that the bubble switches from volumetric to shape oscillations for V greater than 30 V.

The dimensionless amplitude, ξ, of the bubble oscillation (scaled by the bubble radius, R_b) is extracted from single bubble oscillation videos of Exp B and is plotted as a function of f for given V in Fig. 5 (a). The plot shows that the oscillation amplitude generally increases with V but varies nonlinearly with f. We divide the plot into four different regimes depending on the behavior of ξ as a function of voltage, which is explained in more details in Section 3.3. In particular, the acoustic bubble exhibits resonant behavior around $f = 21$ kHz and 35 kHz, which matches the device resonance shown in Fig. 5 (b). The bubble resonant behavior appears to intensify with V at $f = 35$ kHz, as the bubble switches from volumetric to shape oscillations for V greater than 30 V. In this study, we will only focus on the effect of volumetric oscillations on particles and neglect the data range for $V >$30 V at 35 kHz.

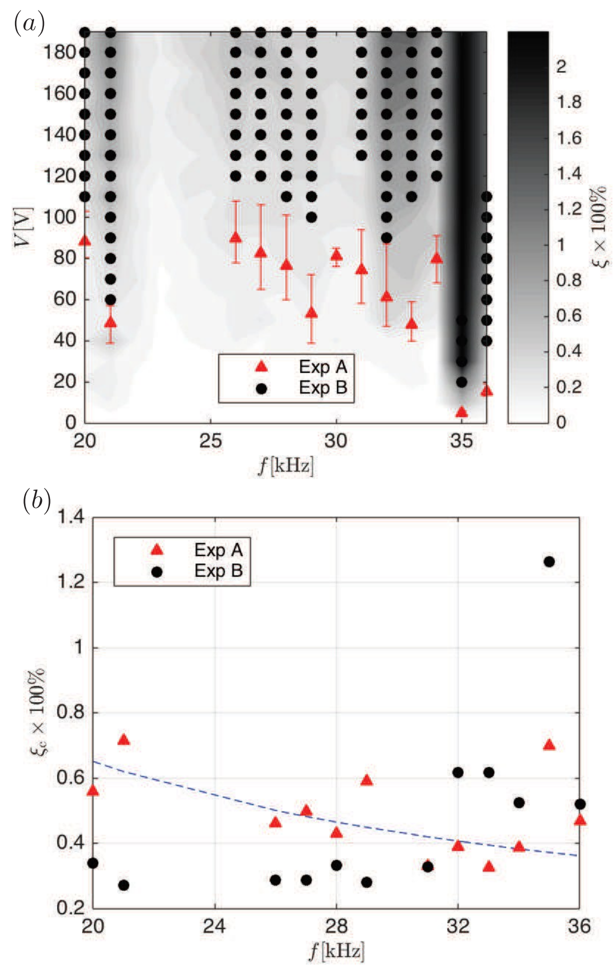

Fig. 6 (a) Phase diagram of experiment results from Exp A and B. The triangular markers represent the voltages at which the particles are released, while the dot markers correspond to particle trapping. The gray scale map gives the magnitude of the oscillation amplitude ξ of the bubble from Exp B. (b) Critical oscillation amplitude ξ_c as a function of frequency f, with the empirical fit to Exp A as a dashed line.

The results of particle and bubble interaction data are summarized in a f-V phase diagram of Fig. 6 (a): The triangular markers indicate the critical voltages for given f at which the particles are released from the bubble (Exp A), while the dots mark the frequencies and voltages at which the particles are trapped and remain on the bubble surface (Exp B). While the threshold release voltages are consistently lower than the minimum trapping voltages, they follow the same general trend for varying f. In addition, no particle trapping and subsequent release are observed between 22 kHz and 25 kHz, as well as at 30 kHz for both experimental sets.

The phase diagram is overlaid with the gray scale map of ξ from Exp B, to show the correlation between the oscillation amplitudes and bubble's ability to trap particles. We observe that the dot markers (trapped particle) tend to appear in the regime where the oscillation amplitude is higher than 0.2 %. The critical bubble amplitudes, ξ_c, at the onset of particle releasing or trapping are plotted as a function of f in Fig. 6 (b). Except for $f = 35$

kHz, most values of ξ_c fall in the range between 0.2%-0.8%.

3.2 Critical Secondary Radiation Force

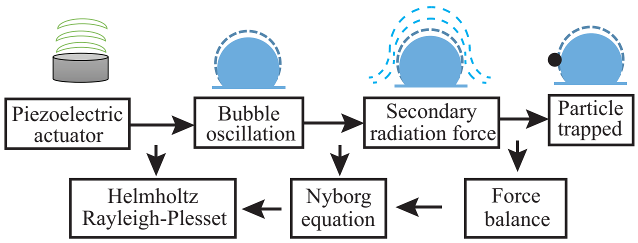

Fig. 7 Flow chart of the working mechanism and corresponding theory for particle trapping. Upon the piezoelectric actuation, the bubble oscillates in response to acoustic pressure waves, and, in turn, generates a secondary radiation force, F_{SR}. The bottom row includes mathematical models that inform each physical process.

The qualitative physical mechanism (from acoustic actuation to bubble oscillation) behind particle trapping via an acoustic bubble is summarized in the flow chart of Fig. 7 (top row). In order to derive the critical input voltage, V_c, that leads to particle trapping for given f, each stage of the flow chart is considered *quantitatively* by employing the following three steps (Fig. 7 bottom row): first, force balance between the attractive secondary radiation force and the net hydrodynamic force on the particle to derive the critical bubble oscillation, ξ_c; second, linearized Rayleigh-Plesset equation to solve for the critical pressure, p'_c, needed to generate ξ_c; finally, reduced Helmholtz equation to relate p'_c to the critical applied voltage, V_c, to address the current lack of direct pressure measurement inside the microchannel. Details of each quantitative analysis are included in Sections 3.2 & 3.3, culminating in the plot of V_c at given f (Fig. 9 (b)) in good agreement with experimental data.

The secondary radiation force, F_{SR}, refers to the near-field attractive or repulsive force between the bubble and an object due to the pressure waves generated by the oscillating bubble[40]. The initial theoretical development of the secondary radiation force was made by Nyborg[76] who derived the following expression for F_{SR},

$$F_{SR} = 4\pi\rho_l \left(\frac{\rho_p - \rho_l}{\rho_l + 2\rho_p}\right) \frac{R_b^6 R_p^3}{d^5} \omega^2 \xi^2, \tag{1}$$

where ρ_l and ρ_p are the liquid and particle densities, respectively; R_p corresponds to the particle radius, and d is the center-to-center distance between the bubble and particle; $\omega = 2\pi f$ is the radian frequency. Doinikov[77,80–82] extended the work of Nyborg to derive a more general expression for F_{SR}, which reduces to Eq. (1) in the limit of $R_p/d \ll 1$. In our current experiments, $R_p/d \sim 0.1$, so that the expression by Nyborg is valid. Here, the primary acoustic radiation force generated by the vibrating microchannel itself is neglected, as the wavelength of the acoustic pressure in our case ($\sim$ 60 mm) is much greater than the channel height (1.35 mm) and yields no spatial pressure gradient[83].

To isolate the effects of F_{SR} from all other forces acting on the particle, the flow rate is fixed at 4 mL/min, so that the mean channel velocity, u_e, is an order of magnitude greater than the characteristic microstreaming velocity[73], $u_s = \xi^2 R_b \omega$. As the effects of microstreaming flows can be neglected in our current setup[84,85], with $u_e/u_s \sim O(10^1)$, the hydrodynamic effects on the particle are independent of the input voltage and frequency and only vary as a function of the particle's location with respect to the bubble. Furthermore, as shown in Fig. 8 (a), the release location of the particle is observed to match the stagnation point of the bubble for all frequencies, ensuring that the net hydrodynamic force on the particle, F_D, must be constant for Exp A, while the particle trapping location in Exp B varies between experimental runs. Therefore, for the sake of simplicity, all the theoretical consideration from hereon will be limited to Exp A.

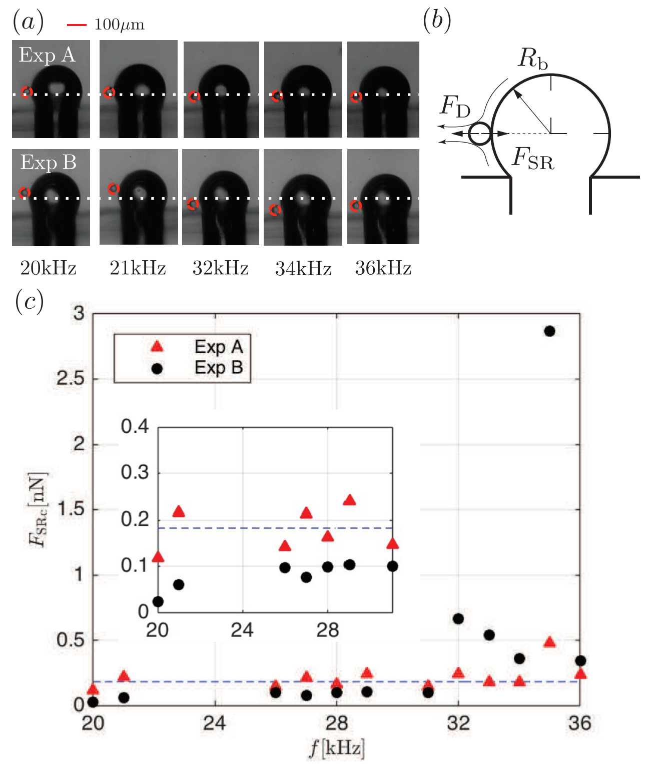

Fig. 8 (a) Images showing the particle location at the onset of release (Exp A) and trapping (Exp B). The top row confirms that the particles is consistently released from the bubble stagnation point, while the bottom row images indicate the particle location upon trapping varies with frequency. (b) Schematic of a particle located at the bubble stagnation point. The secondary radiation force, F_{SR}, must balance the hydrodynamic force, F_D, that tends to pull the particle off the bubble surface. (c) Critical secondary radiation force F_{SRc} as a function of frequency f. The values for F_{SR} for Exp A appear constant, corresponding to the consistent release location. The zoom-in plot shows the values from 20 kHz to 30 kHz. By contrast, the values of F_{SRc} for Exp B shows dependency on f.

Based on a simple force balance depicted in Fig. 8 (b), in the critical moment of particle release from the stagnation point, F_D must balance the threshold secondary radiation force, F_{SRc}, needed to hold the particle on the bubble (*i.e.*, if $F_{SR} < F_{SRc}$, the particle is released from the bubble). By plugging in the experimental values of ξ_c in Eq. (1), F_{SRc} is calculated and plotted in Fig. 8 (c) to reveal that F_{SRc} is indeed constant for Exp A (triangle), as $F_{SRc} = F_D =$ constant. On the other hand, F_D can be estimated by considering a modified Stokes drag on a sphere (*i.e.*, micro-particle) experiencing a local straining flow near the stagnation point of another spherical obstacle (*i.e.*, bubble). Valid in the limit of $R_p/R_b \ll 1$, Goren and O'Neill[86] derived the expression for this modified drag as

$$F_D = 6\pi f_0 \mu U_\infty \left(\frac{R_p}{R_b}\right)^2 R_p, \tag{2}$$

where U_∞ is the external flow velocity at infinity, and μ is the liquid viscosity; f_0 is the correction factor that varies with the particle distance from the obstacle. While this expression has been derived for a solid obstacle that satisfies no slip boundary condition on the surface, it is reasonable to assume that the same functional relationship will hold for a bubble as an obstacle but with a different value of f_0.

Finally, by balancing F_{SR_c} (Eq. (1)) with F_D (Eq. (2)), we can derive an expression for ξ_c upon particle release,

$$\xi_c = \sqrt{\frac{3\mu U_\infty f_0(\rho_l + 2\rho_p)d^5}{2R_b^8 \rho_l(\rho_p - \rho_l)\omega^2}}, \tag{3}$$

where the value of correction factor, f_0, is found by empirically fitting Eq. (3) to data in Fig. 6 (b). This allows us to quantify how the threshold bubble oscillation must depend on different physical parameters of the system, in particular, the driving frequency, f.

3.3 Threshold Acoustic Parameter

For isotropic, volumetric bubble oscillations, the relationship between the resultant oscillation amplitude and driving pressure is given by the Rayleigh-Plesset equation[87,88],

$$R\ddot{R} + \frac{3}{2}\left(\dot{R}\right)^2 = \frac{1}{\rho_l}\left(p_g - p - 4\mu\frac{\dot{R}}{R} - \frac{2\sigma}{R}\right) \tag{4}$$

where R is the instantaneous bubble radius as a function of time and the overhead dot refers to differentiation with respect to time. Here, p_g and p correspond to the internal and external driving pressures of the bubble, respectively, while σ is the surface tension of the water/air interface. Since the bubble oscillation amplitude in our experiments is less than 1%, we may linearize the Rayleigh-Plesset equation by assuming $R = R_0 + R'$ and $p = p_0 + p'$, where R' and p' are the small perturbations of the bubble radius and driving pressure (*i.e.*, $R'/R_0 \ll 1$ and $p'/p_0 \ll 1$). The solution to the linearized Rayleigh-Plesset equation yields a linear relationship between p' and R':

$$p' = R'/G, \tag{5}$$

where

$$G = \frac{R_b^2}{\sigma}\left[\frac{Re_b}{Ca_b}\right]^2 \left\{\frac{We_b - H}{16(4 - \frac{Re_b}{Ca_b}H) - \left[\frac{Re_b}{Ca_b}(H - We_b) - 8\right]^2}\right\}, \tag{6}$$

and

$$H = \frac{3\gamma p_0 R_b}{\sigma} - 2 + 6\gamma, \tag{7}$$

with $\gamma = 1.4$ as the gas constant. Here we define Reynolds number, $Re_b = \rho_l R_b(R_b\omega)/\mu$, capillary number, $Ca_b = \mu(R_b\omega)/\sigma$, and Weber number, $We_b = \rho_l(\omega R_b)^2 R_b/\sigma$, specific to the acoustic bubble, respectively. Since $R'_c = \xi_c R_b$, Eq. (5) allows us to solve for the critical driving pressure, $p'_c = R'_c/G$.

The pressure field generated by the acoustic actuation of the device can be solved based on the Helmholtz equation,[89],

$$\nabla^2 p' + k^2 p' = 0, \tag{8}$$

where the wave number k is given by $k \sim \omega/c_a$, and c_a is the speed of sound in water. In the case of one-dimensional propagation of pressure waves, the solution to the Helmholtz equation is given by

$$p' = i{c_a}^2 \rho_l kl \frac{\sin(kx)}{\cos(kh)} e^{-i\omega t}, \tag{9}$$

where l is the device vibration amplitude. For simplicity, the device amplitude is assumed to increase linearly with V, or $l = K l_{ref} V/V_{ref}$, where l_{ref} is the reference device amplitude at 3 V shown in Fig. 5 (b), and K is the fitting parameter whose value depends on the voltage regime. Since $kx \ll 1$ and $kh \ll 1$, we use the Taylor expansion to further simplify p' to

$$p' = K4\pi^2 \rho_l f^2 h l_{ref}\left(\frac{V}{V_{ref}}\right), \tag{10}$$

where h is the channel half-height.

Finally, combining Eq. (3), (5), (10) leads to the expression for the critical voltage that leads to particle release at given frequency:

$$\frac{V_c}{V_{ref}} = \frac{1}{J(f)}\frac{\sqrt{6}}{4\pi}\sqrt{f_0 U_\infty}\sqrt{\frac{1}{Re_h}}\sqrt{\frac{2\rho_p + \rho_l}{\rho_p - \rho_l}}\left[\frac{R_p}{R_b} + 1\right]^{\frac{5}{2}}\sqrt{\frac{R_b}{h}}, \tag{11}$$

where

$$J(f) = KGl_{ref}We_b f. \tag{12}$$

Each term in $J(f)$ is a function of the excitation frequency, f; here we define alternate Reynolds number with respect to the micro-channel as $Re_h = \rho_l U_\infty h/\mu$. This theoretical function of critical voltage must depend on the experimental parameters (*i.e.*, the particle and bubble radii). For instance, V_c is shown to decrease with increasing channel height, h. The quantification of V_c for particle release and trapping via an acoustic bubble will allow for the optimization of lab on a chip operating conditions to trap or sort micro-sized objects.

The value of the fitting parameter, K, that relates the device amplitude to the bubble amplitude, or the driving pressure, can be extracted by calculating the pressure, p', based on Eq. (5) for varying V. The corresponding dimensionless plot is shown in Fig. 9 (a), which clearly exhibits four different voltage regimes for varying f. In regimes I, II, and IV, the pressure increases in an approximately linear fashion with the voltage at different rates, or K, while the pressure varies nonlinearly with the voltage in regime III. By plugging in the empirical values of K into Eq.(11), we plot the critical voltage V_c for varying f (dashed line) on the experimental phase diagram in Fig. 9 (b), in particularly good agreement with Exp A. Notably, our current theoretical result can

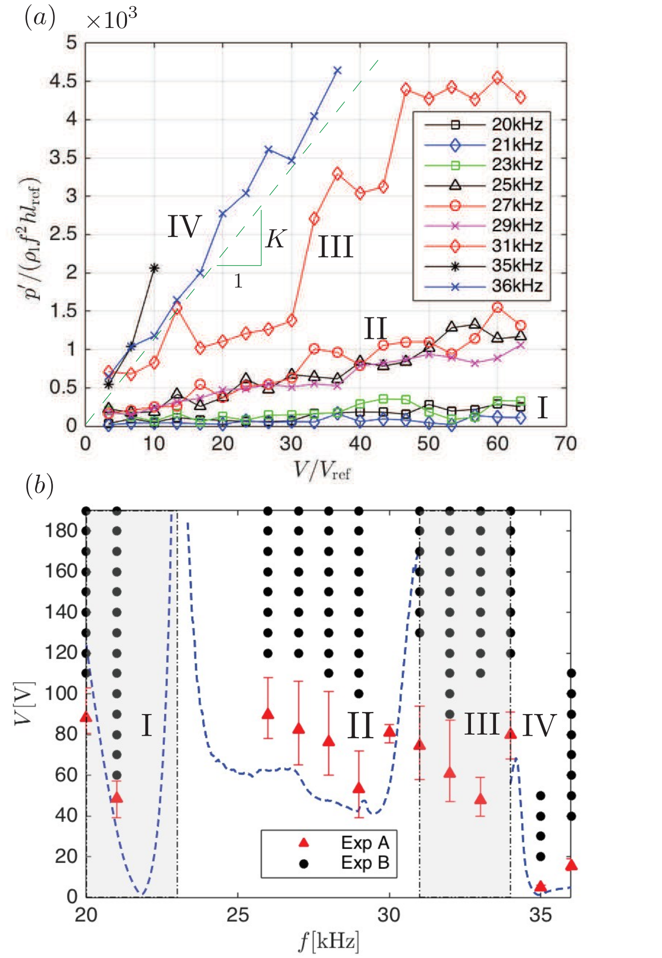

Fig. 9 (a) Dimensionless pressure $p'/(\rho_l f^2 h l_{\mathrm{ref}})$ as a function of voltage V/V_{ref}. The pressure increases in an approximately linear fashion in regime I, II and IV at different rates, K, while the pressure increases nonlinearly in regime III. (b) The dashed curve corresponds to the theoretical result, V_c (Eq. (11)),based on the empirical values of K.

be easily extended to other acoustic devices by simply updating the reference device vibration amplitude l_{ref} and K in Eq. (12) to match the particular experimental setup.

4 Conclusions

In summary, we have hereby quantified the secondary radiation force, F_{SR}, of an acoustic bubble used to trap micro-objects in lab on a chip systems, by combining experiments and reduced modeling. Experimentally, we measure the minimum input voltage at given f needed for a single acoustic bubble to generate sufficient F_{SR} to trap and stabilize a microsphere entrained in flow. This critical voltage is experimentally tested in two ways: by recording the maximum voltage at which an already attached particle is released from the bubble (Exp A) and the minimum voltage at which a particle entrained in flow is first trapped by the oscillating bubble (Exp B), as summarized in a phase diagram. For all experiments, the flow rate of water containing particle suspensions is kept constant and sufficiently high so that the effects of microstreaming flows can be neglected in our current study. In addition to measuring the onset behavior, the amplitude of bubble oscillation is also measured at the corresponding voltages and frequencies to verify the relationship between the oscillation amplitude and F_{SR}, as given by Nyborg[76].

In parallel to experiments, we combine well-developed theories to derive an expression for the critical input voltage that leads to the particle release into the external flow. By balancing the hydrodynamic force on a sphere near a stagnation point[86] with F_{SR}, a functional relationship between the threshold bubble oscillation and experimental parameters, such as particle size and driving frequency, is derived. Then, linearized Rayleigh-Plesset and Helmholtz equations are employed to connect this threshold bubble amplitude to the driving pressure, then to the applied voltage. Aided by empirical parameters to determine the vibration amplitude of the channel, the resultant expression for the critical voltage, V_c, is an explicit function of the driving frequency, f, and is in good quantitative agreement with the data from Exp A. While the final result, $V_c(f)$, has been tested for our particular experimental setup, its theoretical approach and result should be valid for a wide range of acoustic devices and can easily accommodate them by adjusting the device vibration amplitude.

Overall, our work here takes an initial step to quantitatively analyze the secondary radiation force of an acoustic bubble for particle trapping and release in a flow. Therefore, this work paves the way towards future design of next-generation acoustic-based lab on a chip devices for more versatile applications. Future work includes developing a better mathematical model for the hydrodynamic forces on the particle near the oscillating bubble surface. On the experimental side, performing the analogous experiments with a wide range of particle and bubble sizes and measuring the pressure field based on PIV (Particle Image Velocimetry)[90] will help validate our current model. Furthermore, extending this work to include multiple bubbles, microstreaming effects, or non-spherical objects is also of great practical interest for lab on a chip applications.

5 Acknowledgment

This research has been supported by a DARPA Young Faculty Award through grant N66001-11-1-4127. YC and SL thank Dr. Sascha Hilgenfeldt (UIUC) for fruitful discussions and Dr. Tony Yu for help with image processing. The authors would also like to acknowledge Dr. Feng Zhao (WSUV) for resonant frequency measurements and Saadat-Moghaddam for his help with experiments. BM thanks the support from WSUV ENCS Undergraduate Summer Research Program.

References

1 G. M. Whitesides, *Nature*, 2006, **442**, 368–73.
2 H. Stone, A. Stroock and A. Ajdari, *Annual Review of Fluid Mechanics*, 2004, **36**, 381–411.
3 D. Figeys and D. Pinto, *Analytical Chemistry*, 2000, **72**, 330 A–335 A.
4 S. Haeberle and R. Zengerle, *Lab on a chip*, 2007, **7**, 1094–110.
5 K.-i. Ohno, K. Tachikawa and A. Manz, *Electrophoresis*, 2008, **29**, 4443–53.

6 D. B. Weibel and G. M. Whitesides, *Current opinion in chemical biology*, 2006, **10**, 584–91.

7 D. J. Beebe, G. a. Mensing and G. M. Walker, *Annual review of biomedical engineering*, 2002, **4**, 261–86.

8 J. Wang, L. Ren, L. Li, W. Liu, J. Zhou, W. Yu, D. Tong and S. Chen, *Lab on a chip*, 2009, **9**, 644–52.

9 J. Pihl, M. Karlsson and D. T. Chiu, *Drug discovery today*, 2005, **10**, 1377–83.

10 P. S. Dittrich and A. Manz, *Nature reviews. Drug discovery*, 2006, **5**, 210–218.

11 R. Barry and D. Ivanov, *Journal of nanobiotechnology*, 2004, **2**, 2.

12 L. Guo, J. Feng, Z. Fang, J. Xu and X. Lu, *Trends in Food Science & Technology*, 2015.

13 L. Marle and G. M. Greenway, *Trends in Analytical Chemistry*, 2005, **24**, 795–802.

14 J. Voldman, *Annual review of biomedical engineering*, 2006, **8**, 425–54.

15 D. Kohlheyer, J. C. T. Eijkel, A. van den Berg and R. B. M. Schasfoort, *Electrophoresis*, 2008, **29**, 977–93.

16 M. Dürr, J. Kentsch, T. Müller, T. Schnelle and M. Stelzle, *Electrophoresis*, 2003, **24**, 722–31.

17 P. Li, N. Lei, J. Xu and W. Xue, *IEEE Transactions on Nanotechnology*, 2012, **11**, 751–759.

18 H. Shafiee, J. L. Caldwell, M. B. Sano and R. V. Davalos, *Biomedical microdevices*, 2009, **11**, 997–1006.

19 K. H. Kang, Y. Kang, X. Xuan and D. Li, *Electrophoresis*, 2006, **27**, 694–702.

20 N. Pamme, J. C. Eijkel and A. Manz, *Journal of Magnetism and Magnetic Materials*, 2006, **307**, 237–244.

21 H. H. Bau, J. Zhong and M. Yi, *Sensors and Actuators B: Chemical*, 2001, **79**, 207–215.

22 M. a. M. Gijs, *Microfluidics and Nanofluidics*, 2004, 22–40.

23 T. Zhu, R. Cheng, Y. Liu, J. He and L. Mao, *Microfluidics and Nanofluidics*, 2014, **17**, 973–982.

24 M. Ozkan, M. Wang, C. Ozkan, R. Flynn and S. Esener, *Biomedical Microdevices*, 2003, 61–67.

25 F. Arai, C. Ng, H. Maruyama, A. Ichikawa, H. El-Shimy and T. Fukuda, *Lab on a chip*, 2005, **5**, 1399–403.

26 H. Zhang and K.-K. Liu, *Journal of the Royal Society Interface*, 2008, **5**, 671–90.

27 F. Gallaire, C. N. Baroud, J.-P. Delville and Others, *International Journal of Heat and Technology*, 2008, **26**, 161–166.

28 A. Darhuber, J. Valentino, S. Troian and S. Wagner, *Journal of Microelectromechanical Systems*, 2003, **12**, 873–879.

29 R. D. Johnson, I. H. A. Badr, G. Barrett, S. Lai, Y. Lu, M. J. Madou and L. G. Bachas, *Analytical Chemistry*, 2001, **73**, 3940–3946.

30 R. Gorkin, J. Park, J. Siegrist, M. Amasia, B. S. Lee, J.-M. Park, J. Kim, H. Kim, M. Madou and Y.-K. Cho, *Lab on a chip*, 2010, **10**, 1758–73.

31 H. Bruus, J. Dual, J. Hawkes, M. Hill, T. Laurell, J. Nilsson, S. Radel, S. Sadhal and M. Wiklund, *Lab on a chip*, 2011, **11**, 3579–80.

32 J. Friend and L. Y. Yeo, *Reviews of Modern Physics*, 2011, **83**, 647–704.

33 S.-C. S. Lin, X. Mao and T. J. Huang, *Lab on a chip*, 2012, **12**, 2766–70.

34 L. Y. Yeo and J. R. Friend, *Biomicrofluidics*, 2009, **3**, 12002.

35 G. Yu, X. Chen and J. Xu, *Soft Matter*, 2011, **7**, 10063.

36 A. Lenshof, C. Magnusson and T. Laurell, *Lab on a chip*, 2012, **12**, 1210–23.

37 S. M. Hagsäter, T. G. Jensen, H. Bruus and J. P. Kutter, *Lab on a chip*, 2007, **7**, 1336–44.

38 P.-H. Huang, Y. Xie, D. Ahmed, J. Rufo, N. Nama, Y. Chen, C. Y. Chan and T. J. Huang, *Lab on a chip*, 2013, **13**, 3847–52.

39 A. Hashmi, G. Yu, M. Reilly-Collette, G. Heiman and J. Xu, *Lab on a chip*, 2012, **12**, 4216–27.

40 Y. Chen and S. Lee, *Integrative and comparative biology*, 2014, **54**, 959–68.

41 W. Lauterborn and T. Kurz, *Reports on Progress in Physics*, 2010, **73**, 106501.

42 B. Tran, T. Hall, J. Fowlkes and C. Cain, *IEEE Transactions on Ultrasonics, Ferroelectrics and Frequency Control*, 2003, **50**, 1296–1304.

43 Y. Liu, H. Yang and A. Sakanishi, *Biotechnology advances*, 2006, **24**, 1–16.

44 N. Smith, *International journal of nanomedicine*, 2007, **2**, 585–594.

45 W. D. O'Brien, *Progress in biophysics and molecular biology*, 2007, **93**, 212–55.

46 J. Xu and D. Attinger, *Physics of Fluids*, 2007, **19**, 108107.

47 D. Hsieh, *The Journal of the Acoustical Society of America*, 1974, **56**, 392–393.

48 S. A. Elder, *The Journal of the Acoustical Society of America*, 1959, **31**, 54.

49 P. Tho, R. Manasseh and A. Ooi, *Journal of Fluid Mechanics*, 2007, **576**, 191.

50 J. Xu and D. Attinger, *Journal of Micromechanics and Microengineering*, 2007, **17**, 609–616.

51 L. A. Crum, *The Journal of the Acoustical Society of America*, 1975, **57**, 1363.

52 P. Rogers and A. Neild, *Lab on a chip*, 2011, **11**, 3710–5.

53 S. K. Chung and S. K. Cho, *Journal of Micromechanics and Microengineering*, 2008, **18**, 125024.

54 S. K. Chung and S. K. Cho, *Microfluidics and Nanofluidics*, 2008, **6**, 261–265.

55 Y. Xu, A. Hashmi, G. Yu, X. Lu, H.-J. Kwon, X. Chen and J. Xu, *Applied Physics Letters*, 2013, **102**, 023702.

56 P. Marmottant and S. Hilgenfeldt, *Proceedings of the National Academy of Sciences of the United States of America*, 2004, **101**, 9523–7.

57 P. Marmottant, M. Versluis, N. de Jong, S. Hilgenfeldt and D. Lohse, *Experiments in Fluids*, 2005, **41**, 147–153.

58 Y. Xie, D. Ahmed, M. I. Lapsley, M. Lu, S. Li and T. J. Huang, *Journal of laboratory automation*, 2014, **19**, 137–43.

59 A. Hashmi, G. Heiman, G. Yu, M. Lewis, H.-J. Kwon and J. Xu, *Microfluidics and Nanofluidics*, 2012, **14**, 591–596.

60 A. Ozcelik, D. Ahmed, Y. Xie, N. Nama, Z. Qu, A. A. Nawaz and T. J. Huang, *Analytical chemistry*, 2014, **86**, 5083–8.

61 A. R. Tovar, M. V. Patel and A. P. Lee, *Microfluidics and Nanofluidics*, 2011, **10**, 1269–1278.

62 A. R. Tovar and A. P. Lee, *Lab on a chip*, 2009, **9**, 41–3.

63 M. V. Patel, A. R. Tovar and A. P. Lee, *Lab on a chip*, 2012, **12**, 139–45.

64 P.-H. Huang, M. Ian Lapsley, D. Ahmed, Y. Chen, L. Wang and T. Jun Huang, *Applied physics letters*, 2012, **101**, 141101.

65 J. Kao, X. Wang, J. Warren, J. Xu and D. Attinger, *Journal of Micromechanics and Microengineering*, 2007, **17**, 2454–2460.

66 D. Ahmed, C. Y. Chan, S.-C. S. Lin, H. S. Muddana, N. Nama, S. J. Benkovic and T. J. Huang, *Lab on a chip*, 2013, **13**, 328–31.

67 J. M. Won, J. H. Lee, K. H. Lee, K. Rhee and S. K. Chung, *International Journal of Precision Engineering and Manufacturing*, 2011, **12**, 577–580.

68 J. Feng and S. K. Cho, 2013 IEEE 26th International Conference on Micro Electro Mechanical Systems (MEMS), 2013, pp. 63–66.

69 S. Hagsater, A. Lenshof, P. Skafte-Pedersen, J. Kutter, T. Laurell and H. Bruus, *Lab on a Chip*, 2008, **8**, 1178–1184.

70 P. Marmottant and S. Hilgenfeldt, *Nature*, 2003, **423**, 153–156.

71 C. Wang, B. Rallabandi and S. Hilgenfeldt, *Physics of Fluids*, 2013, **25**, 022002.

72 P. Marmottant and S. Hilgenfeldt, *PNAS*, 2004, **101**, 9523–9527.

73 P. Marmottant, J. Raven, H. Gardeniers, J. Bomer and S. Hilgenfeldt, *Journal of Fluid Mechanics*, 2006, **568**, 109–118.

74 P. Marmottant, T. Biben and S. Hilgenfeldt, *Proceedings of the Royal Society A: Mathematical, Physical and Engineering Sciences*, 2008, **464**, 1781–1800.

75 B. Rallabandi, C. Wang and S. Hilgenfeldt, *Journal of Fluid Mechanics*, 2014, **739**, 57–71.

76 W. Nyborg, *Acoustic Society of America*, 1967.

77 S. Z. A.A. Doinikov, *Ultrasonic*, 1996, **34**, 807–815.

78 A. N. Priscilla Rogers, *Lab on a Chip*, 2011, **11**, 3710–3715.

79 X. Huang, W. Hui, C. Hao, W. Yue, M. Yang, Y. Cui and Z. Wang, *Small*, 2014, **10**, 758–765.

80 A. A. Doinikov, *Journal of Fluid Mechanics*, 2001, **444**, 1–21.

81 A. A. Doinikov, in *Recent Research Development of Acoustics*, Transworld Research Network, 2003, vol. 1, ch. 3, pp. 39–67.

82 A. A. Doinikov, in *Bubble and Particle Dynamics in Acoustic Fields: Modern Trends and Applications*, ed. A. A. Doinikov, Research Signpost, 2005, ch. Bjerknes forces and translational bubble dynamics, pp. 95–143.

83 T. G. Leighton, *The Acoustic Bubble*, Academic Press, 1994.

84 C. Wang, S. V. Jalikop and S. Hilgenfeldt, *Biomicrofluidics*, 2012, **6**, year.

85 C. Wang, S. V. Jalikop and S. Hilgenfeldt, *Applied Physics Letters*, 2011, **99**, year.

86 S. L. Goren and M. E. O'Neill, *Chemical Engineering Science*, 1971, **26**, 325 – 338.

87 M. P. Brenner, S. Hilgenfeldt and D. Lohse, *Reviews of Modern Physics*, 2002, **74**, 425–484.

88 C. E. Brennen, *Cavitation and Bubble Dynamics*, Cambridge University Press, 1995, p. 282.

89 H. Bruus, in *Theoretical Microfluidics*, ed. H. Bruus, Oxford University Press, 2008, ch. Acustofluidics.

90 B. W. van Oudheusden, *Measurement Science and Technology*, 2013, **24**, year.